An accelerated level-set method for inverse scattering problems

Lorenzo Audibert, Houssem Haddar, Xiaoli Liu

▶ **To cite this version:**

An accelerated level-set method for inverse scattering problems

Lorenzo Audibert[*]   Houssem Haddar[†]   Xiaoli Liu[‡]

Abstract

We propose a rapid and robust iterative algorithm to solve inverse acoustic scattering problems formulated as a PDE constrained shape optimization problem. We use a level-set method to represent the obstacle geometry and propose a new scheme for updating the geometry based on an adaptation of accelerated gradient descent methods. The resulting algorithm aims at reducing the number of iterations and improving the accuracy of reconstructions. To cope with regularization issues, we propose a smoothing to the shape gradient using a single layer potential associated with ik where k is the wave number. Numerical experiments are given for several data types (full aperture, backscattering, phaseless, multiple frequencies) and show that our method outperforms a non accelerated approach in terms of convergence speed, accuracy and sensitivity to initial guesses.

Keywords: inverse scattering problem, shape optimization, level-set method, Nesterov accelerated gradient.

1   Introduction

We are interested in inverse acoustic obstacle scattering problems with far field measurements. Motivated by applications, several types/settings of the data are considered, such as full or partial far field data, backscattering data, phaseless data and multiple frequency data. The corresponding inverse problems are put in an unified framework of a PDE constrained shape optimization problem. To fix ideas, we restrict ourselves to Dirichlet obstacles but the methodology can be easily extended to other models of scattering problems.

Many inversion algorithms have been developed for this inverse problem and we can refer to [12, 13] for recent overviews of different class of methods to solve this severely ill posed problem. Roughly speaking, for a qualitative and fast imaging methods one can rely on linearization approaches as in [3, 4] and the references therein or sampling methods as in [5, 10, 23] and the references therein. A computationally more involved but potentially more accurate reconstruction methods, which we are going to

---

[*]EDF R&D PRISME, 78400, Chatou, France (`lorenzo.audibert@edf.fr`)

[†]INRIA and Ecole Polytechnique (CMAP), Institut Polytechnique de Paris, Route de Saclay, 91128, Palaiseau, France (`houssem.haddar@polytechnique.edu`)

[‡]Corresponding author. INRIA and Ecole Polytechnique (CMAP), Institut Polytechnique de Paris, Route de Saclay, 91128, Palaiseau, France (`xiaoli.liu@polytechnique.edu`)

discuss in this paper, are based on the inversion of the full model, by either reformulating the inverse problem as a PDE constrained shape optimization problem (see for instance [8] in the context of inverse scattering problems) or using a Newton-type technique (the literature is richer in inverse scattering community and we synthetically refer to [12, 22, 18, 20] and references therein). The latter is a tool of choice if one possesses a reliable predefined parametrization of the geometry with a relatively small number of parameters to preserve computational effectiveness. In the case of large parameters, regularization of the Jacobian matrix is needed leading to inexact Newton methods. We refer to [25] for the analysis of this type of methods. When the pseudo inverse is approximated with few iterations of a conjugated gradient method, the adjoint state can advantageouly be used to speed up iterations [11, 18]. Although not theoretically proved, due to regularization issues, these methods usually require a relatively small number of iterations to achieve reasonable accuracy.

We here adopt a more flexible approach based on reformulating the problem as the minimization of a least squares cost functional using a gradient descent. The main advantage is that, thanks to the use of adjoint state technique, the iteration cost is relatively cheap and is independent from the number of parameters of the inverse problem. One therefore does not need a predefined parametrization of the geometry. This method can also be naturally coupled with a level set parametrization of the unknown shape, offering the possibility of encoding a complex topology. In the context of inverse scattering and level-set method we refer to the review article [14] and the seminal work [37]. The approach we use here is inspired by the one developed for shape optimization problems in [1]. The main drawback of the gradient descent method is that it usually requires a large number of iterations before achieving a reasonable accuracy. Some adaptation of the step size using line search technique for instance can be helpful in improving this performance. It is also numerically observed that the level-set method tends to reduce the complexity of the topology during iterations (merging connected components rather than creating new ones). Our main goal here is to propose a way to improve these shortcomings based on gradient descent acceleration techniques. Let us first notice that other approaches to accelerate the level set methods have been proposed in the literature, such as Kaczmarz type gradient-based descent directions in [15], stochastic gradient descent, the Adam method and a stochastic quasi-Newton scheme in [19]. We do not intent to compete with these approaches but rather present a different possibility.

About forty years ago, Nesterov proposed an accelerated gradient method in [30] and its wide success stimulated the development of many first-order acceleration variants (for an unified analysis of these works see [40] and for a review see [31]). The Nesterov acceleration has been analyzed for inverse parameters problems in [32]. We are interested here in the application of this technique to shape inverse problems which, to the best of our knowledge, has not been addressed in the literature. The main difficulty is to give an interpretation to the Nesterov scheme in the space of parametrization free shapes, which is not endowed with a Hilbert structure for example. The proposed algorithm is as follows. At each iteration, we first use the shape derivative to solve the Hamilton-Jacobi equation and get a new update of the level-set function. For a classical gradient method, this new level-set function is viewed as the representation of the obstacle shape for the next step. In the accelerated algorithm, we rather make

a suitable combination of this new level-set function with the previous one to get the representation of the obstacle for the next step. More precisely, we apply the Nesterov rule for choosing the weights to the signed distance functions (derived from the level set function) at each step. We explain in a simplified $1D$ example why the use of the sign distance function is a natural way to implement the acceleration rule. A rigorous theoretical justification of this approach is still under study and is faced with the difficulty of relating the shape gradient to the derivative in the topology endowed by sign distance metric: the distance between two shapes is measured by the L^2 norm of the difference between associated sign distances. The scope of the current work is purely numerical and intends to demonstrate the numerical efficiency of the proposed methodology for different scenarios of the inverse problem data.

In the implementation of the numerical scheme, we also consider a new way to regularize and extend the shape gradient. Due to the ill-posedness of the inverse problem, the gradient of the cost functional may produce very irregular descent directions when the number of parameters is large. Two regularization strategies can be adopted to cope with this difficulty. The first one relies on adding a penalty term to the cost functional while the second one relies on regularizing the gradient descent and encoding an early stopping rule. We adopt the latter approach to avoid introducing a bias in the cost functional. This approach also goes well with the level set approach since one needs to define a representative of the shape gradient (which is defined on the boundary of the unknown) on the domain where the level set function lives. Motivated by the use of integral equation method to solve the direct problem, we propose to use a single-layer potential associated with ik where k is the wave number with density equal to the shape gradient. This offers a one order smoothed descent direction with a smoothing width depending on the frequency.

One of the main advantages of the numerical algorithm that we propose is its versatility and the good numerical performances that it provides for different data types. We conduct in these first investigations only two-dimensional experiments inspired by the literature on inverse scattering problems. A comparative study with a non accelerated scheme shows a spectacular improvements in the accuracy and the speed of convergence as well as a much less sensitivity to the topology of the initial guess. One additional observation from our numerical results is that the Nesterov scheme can help escaping small local minima. The possibility of avoiding local minima for inversion schemes applied to inverse scattering problems has been observed in other methods, such as Kaczmarz approach [15] and stochastic gradient descent method [14], which can be viewed as a sub-gradient method, thus can avoid certain local minima when using a cyclic choice of partial data sets for gradient estimation. For strong local minima, as shown in the case of backscattering data, the algorithm may fail and a different initial guess should be used. This is also the case of high frequencies with geometries containing fine details as demonstrated by an example. The use of initial guess from lower frequencies helped solving this shortcoming and acceleration is observed in both steps.

The organization of this paper is as follows. In section 2, we formulate the direct scattering problem and formulate the inverse problem as a PDE constrained shape optimization problem. In Section 3 an

adjoint scattering problem is introduced and is used to derive the shape derivative of a generic cost functional that encompass various data settings. Section 4 is dedicated to the presentation of the accelerated level-set method based on the Nesterov acceleration method. In Section 4.1 a complete description of the inversion algorithm is provided including the regularization scheme for the shape gradient. Finally, the numerical implementation and validation of our algorithm is presented in section 5.

2   The Inverse scattering problem

We here introduce the inverse scattering problem that we take as a model problem and its formulation as a PDE constrained shape optimization problem.

Let $D \subset \mathbb{R}^N$ ($N = 2$ or 3) be an open and bounded domain with C^2-boundary ∂D such that the exterior $\mathbb{R}^N \backslash \overline{D}$ of $\overline{D}$ is connected. Here and throughout the monograph we denote by $\overline{D}$ the closure of the set D of points in $\mathbb{R}^N$. We consider incident plane waves defined as

$$u^i(x; d, k) := e^{ikx \cdot d}, \quad x \in \mathbb{R}^N, \tag{2.1}$$

where $k > 0$ is the wave number and $d \in \mathbb{S}^{N-1}$ is a given incident direction. Here, $\mathbb{S}^{N-1}$ denotes the unit sphere in $\mathbb{R}^N$. The obstacle D gives rise to a scattered field $u^s \in H^1_{loc}(\mathbb{R}^N \setminus \overline{D})$ such that the total field $u = u^i + u^s$ and u^s satisfy

$$\begin{aligned}
\Delta u + k^2 u &= 0 \quad \text{in} \quad \mathbb{R}^N, \\
u &= 0 \quad \text{on} \quad \partial D, \\
\lim_{r \to \infty} r^{\frac{N-1}{2}} \left(\frac{\partial u^s}{\partial r} - iku^s \right) &= 0, \quad r = |x|,
\end{aligned} \tag{2.2}$$

where the latter is the Sommerfeld radiation condition that holds uniformly with respect to $\hat{x} = x/|x|$. It is well-known that a unique solution of this problem exists [29]. For numerical purposes, the scattering problem is reformulated using an integral equation formalism. Given a density function λ, the single-layer potential with density λ is defined as

$$(\mathcal{S}_k \lambda)(x) := \int_{\partial D} \lambda(y) G_k(x, y) ds(y), \quad x \in \mathbb{R}^N \backslash \partial D, \tag{2.3}$$

where G_k is the fundamental solution to Helmholtz equation: $G_k(x, y) = \frac{i}{4} H_0^{(1)}(k|x - y|)$ for $N = 2$ and $G_k(x, y) = \frac{e^{ik|x-y|}}{4\pi|x-y|}$ for $N = 3$. Seeking a solution to (2.2) in the form of $u^s(x) := (\mathcal{S}_k \lambda)(x)$ in $\mathbb{R}^N \setminus \overline{D}$ is equivalent to solving for $\lambda \in H^{-1/2}(\partial D)$

$$\int_{\partial D} \lambda(y) G_k(x, y) ds(y) = -u^i(x), \quad x \in \partial D. \tag{2.4}$$

Assuming that k^2 is not a Dirichlet eigenvalue for $-\Delta$ in D, equation (2.4) is well posed [27]. For the numerical implementation of this boundary integral equation we used the gypsilab toolbox [2] that uses a

first order finite element method applied to a variational writing of (2.4). The radiation condition implies the following behavior at infinity:

$$u^s(x) = \frac{e^{ik|x|}}{|x|^{(N-1)/2}} \left\{ u^\infty(\hat{x}) + O\left(\frac{1}{|x|}\right) \right\}, \quad |x| \to \infty,$$

where u^∞ is the so-called the far field pattern of u^s. It is an analytic function on the unit sphere $\mathbb{S}^{N-1}$ and admits the following representation [12]

$$u^\infty(\hat{x}) = C_N \int_{\partial K_R} \left\{ u^s(y) \frac{\partial e^{-ik\hat{x}\cdot y}}{\partial \nu(y)} - \frac{\partial u^s}{\partial \nu}(y) e^{-ik\hat{x}\cdot y} \right\} ds(y), \quad \hat{x} \in \mathbb{S}^{N-1},$$

where $R > 0$ such that $\overline{D} \subset K_R := \left\{ y \in \mathbb{R}^N \mid |y| < R \right\}$ and $C_N = \frac{e^{i\frac{\pi}{4}}}{\sqrt{8\pi k}}$ for $N = 2$ and $C_N = \frac{1}{4\pi}$ for $N = 3$.

The *inverse scattering problem* that we are interested in is to reconstruct ∂D from a knowledge of data related to the far field pattern u^∞. Some results on uniqueness issues for this problem can be found in [12, Chapter 5] and references therein. We also will consider cases where only the modulus of u^∞ is measured (phaseless data). For uniqueness issues related to this problem we refer for instance to [26].

The inverse problem as a PDE constrained shape optimization problem: As mentioned before we formulate the inverse problem as a PDE constrained shape optimization problem, which aims at minimizing a cost function that depends on ∂D via the solution $u^s(\partial D)$ of the scattering problem (2.2). We shall assume hereafter that D (that may vary during iterations) is always contained in K_R for fixed R. For the inverse problem we will have access to the far field pattern for a set of measurement directions $\hat{x}_m, m = 1, ..., M$ and for eventually several incident plane waves (2.1) with incident directions $d_l, l = 1, ..., L$. We first introduce the pointwise measurement operator operator $H_m : H^2(K_{2R} \setminus K_R) \to \mathbb{C}$ defined by

$$H_m u = C_N \int_{\partial K_R} \left\{ u(y) \frac{\partial e^{-ik\hat{x}_m \cdot y}}{\partial \nu(y)} - \frac{\partial u}{\partial \nu}(y) e^{-ik\hat{x}_m \cdot y} \right\} ds(y), \quad \hat{x} \in \mathbb{S}^{N-1}, \tag{2.5}$$

which is a linear and continuous mapping. In particular $H_m u^s = u^\infty(\hat{x}_m)$ where u^∞ is the far field associated with the scattered field u^s. We make use in the sequel of the notation $u_l^s(\partial D)$ to refer to the scattered field associated to incident plane wave with direction d_l and a Dirichlet obstacle D. Let $D^\star$ be the true obstacle. The exact measurement data for different scenarios can be modeled as

$$f_{lm} := \phi\left(H_m u_l^s(\partial D^\star)\right), \quad m = 1, ..., M, \quad l = 1, ..., L,$$

where ϕ denotes a regular function that will be specified later. The solution $\partial D^\star$ of our inverse problem is then sought as a minimizer over $\mathcal{T}$, the set of boundaries ∂D of C^1 domains D strictly included in K_R with connected complements, of the cost functional

$$J(\partial D) := \frac{1}{2LM} \sum_{l=1}^{L} \sum_{m=1}^{M} \left| \phi\left(H_m u_l^s(\partial D)\right) - f_{lm} \right|^2. \tag{2.6}$$

In the case of noisy data $f_{lm}^\delta = f_{lm} + O(\delta)$, the cost functional is obtained by replacing f_{lm} with f_{lm}^δ. We shall apply a gradient descent method to approximate the optimal shape associated with J. We introduce in next section the adjoint state that allows us to easily express and compute the gradient of this cost functional.

5

3 The shape derivative and adjoint state

The shape differentiation of the functional J depends on the existence of a shape derivative for the scattered fields. The latter has been established in the literature and we shall rely on these results to establish the shape Fréchet differentiablity of J. However, and as classically used in shape optimization problems, one does not use the state shape derivative of the state variable to compute the gradient of J since this would be costly. We rather use an adjoint state to evaluate this derivative. Obtaining the adjoint state equation can be formally derived using the Lagrangian technique. We here use a rather direct approach based on the expression of the shape derivative.

3.1 Shape derivative of the scattered field

For any real vector field $\theta \in C^1(\partial D; \mathbb{R}^N)$, we denote by ∂D_θ the set

$$\partial D_\theta := \{x + \theta(x) \mid x \in \partial D\},$$

which is the boundary of a domain D_θ provided $\|\theta\|_\infty := \max_{x \in \partial D} |\theta(x)| < \eta$ with $\eta > 0$ being small enough. We consider the application $U : \mathcal{T} \to H^2(K_{2R} \setminus K_R)$ that maps ∂D to $u^s(\partial D)|_{K_{2R} \setminus K_R}$ where $u^s(\partial D)$ is the solution of (2.2) and where $\mathcal{T}$ denotes the set of admissible boundaries, in particular all boundaries of the form ∂D_θ with $\|\theta\|_\infty < \eta$.

The mapping U is said to be *shape differentiable* at ∂D if for all $\theta \in C^1(\partial D; \mathbb{R}^N)$,

$$\frac{1}{\|\theta\|_{C^1(\partial D;\mathbb{R}^N)}} \|U(\partial D_\theta) - U(\partial D) - U'(\partial D)(\theta)\|_{H^2(K_{2R} \setminus K_R)} \to 0 \quad \text{as} \quad \theta \to 0, \tag{3.7}$$

where the linear mapping $\theta \mapsto U'(\partial D)(\theta)$ is continuous from $C^1(\partial D; \mathbb{R}^N)$ into $H^2(K_{2R} \setminus K_R)$. This mapping is then the *shape derivative* of U at ∂D.

Rigorous foundations for the Fréchet differentiability including characterizations of the derivative both for the Dirichlet and Neumann boundary condition were given by Kirsch in [22] and Hettlich in [17], respectively. Hettlich [17] also established differentiability for the exterior Robin problem and the transmission problem. Here we focus on the Dirichlet case and present the following results given by Kirsch [22].

Theorem 3.1. *Assume that ∂D is a C^2 boundary, consider a real vector field $\theta \in C^1\left(\partial D; \mathbb{R}^N\right)$ and let $u \in H^1_{\text{loc}}\left(\mathbb{R}^N\right)$ be the solution of the scattering problem (2.2). Then the Fréchet derivative $U'(\partial D)(\theta)$ exists and is equal to $v_\theta|_{K_{2R} \setminus K_R}$, where $v_\theta \in H^1_{\text{loc}}(\mathbb{R}^N \setminus \overline{D})$ solves the exterior boundary value problem*

$$\Delta v_\theta + k^2 v_\theta = 0 \quad in \quad \mathbb{R}^N \setminus \overline{D},$$
$$v_\theta = -\frac{\partial u}{\partial \nu} \nu \cdot \theta \quad on \quad \partial D, \tag{3.8}$$
$$v_\theta \quad s.t. \text{ the radiating condition in (2.2).}$$

Here $\nu(x)$ denotes the outer unit normal at $x \in \partial D$.

3.2 Shape derivative of the cost functional

Similarly to the above, the cost functional $J : \mathcal{T} \to \mathbb{R}$ is said to be *shape differentiable* at ∂D if $\theta \mapsto J(\partial D_\theta)$ from $C^1(\partial D; \mathbb{R}^N)$ into $\mathbb{R}$ is Fréchet-differentiable at 0, i.e., the following expansion holds in the vicinity of 0:

$$J(\partial D_\theta) = J(\partial D) + J'(\partial D)(\theta) + o\left(\|\theta\|_{C^1(\partial D;\mathbb{R}^N)}\right), \tag{3.9}$$

with a continuous linear mapping $\theta \mapsto J'(\partial D)(\theta)$ from $C^1(\partial D; \mathbb{R}^N)$ into $\mathbb{R}$ referred to as the *shape derivative* of J at ∂D.

Now we give the shape derivative of the cost functional (2.6) in the following theorem. We consider functions ϕ defined on $\mathbb{C}$ that are either holomorphic and in that case we denote by $\tilde{\phi} = \phi'$ or ϕ is of the form $\phi(z) = f(|z|^2)$ with real valued C^1 function $f : \mathbb{R}_+ \to \mathbb{R}$ and in that case we set $\tilde{\phi}(z) = 2z f'(|z|^2)$.

Theorem 3.2. *Let $D \subset \mathbb{R}^N$ be a bounded domain of class C^2. Consider the cost functional J defined by (2.6) with ϕ and $\tilde{\phi}$ being defined as above. Then J is shape differentiable at ∂D and its shape derivative is:*

$$J'(\partial D)(\theta) = \frac{1}{L}\mathfrak{R}\sum_{l=1}^{L}\int_{\partial D}\frac{\partial u_l}{\partial \nu}\frac{\partial w_l}{\partial \nu}(\nu \cdot \theta)\,ds, \quad \forall \theta \in C^1\left(\partial D; \mathbb{R}^N\right), \tag{3.10}$$

where u_l is the total field of the scattering problem (2.2) with $d = d_l$ and $w_l := w_l^i + w_l^s$ is the solution to the adjoint problem

$$\begin{aligned}\Delta w_l + k^2 w_l &= 0 \quad in \quad \mathbb{R}^N\backslash\overline{D}, \\ w_l &= 0 \quad on \quad \partial D, \\ w_l^s &\quad \text{s.t. the radiating condition in (2.2),}\end{aligned} \tag{3.11}$$

with

$$w_l^i(y) := \frac{C_N}{M}\sum_{m=1}^{M}R_{lm}(\partial D)e^{-ik\hat{x}_m \cdot y} \quad and \quad R_{lm}(\partial D) := \overline{\left(\phi\left(H_m u_l^s(\partial D)\right) - f_{lm}\right)\tilde{\phi}\left(H_m u_l^s(\partial D)\right)}. \tag{3.12}$$

Proof. We denote by $U_l : \mathcal{T} \to H^2(K_{2R} \setminus K_R), l = 1, ..., L$ the application that maps ∂D to $u_l^s(\partial D)|_{K_{2R}\setminus K_R}$ where $u_l^s(\partial D)$ is the solution of (2.2) corresponding to the incident direction d_l. First observe that if we define

$$j(z) = \frac{1}{2}|\phi(z) - f_{lm}|^2,$$

then $j(z+h) = j(z) + \mathfrak{R}\left(\overline{(\phi(z) - f_{lm})\tilde{\phi}(z)}\,h\right) + o(|h|^2)$. Therefore, due to the existence of $U_l'(\partial D)(\theta)$ shown in Theorem 3.1, by the chain rule, the shape derivative of the cost functional J exists and can be written as, for any $\theta \in C^1\left(\partial D; \mathbb{R}^N\right)$,

$$J'(\partial D)(\theta) = \frac{1}{LM}\mathfrak{R}\sum_{l=1}^{L}\sum_{m=1}^{M}\overline{\left(\phi\left(H_m u_l^s(\partial D)\right) - f_{lm}\right)\tilde{\phi}\left(H_m u_l^s(\partial D)\right)}H_m\left(U_l'(\partial D)(\theta)\right). \tag{3.13}$$

7

Also by Theorem 3.1, we know that $U'_l(\partial D)(\theta)$ is the scattered field $v_{\theta,l}(x)$ for problem (3.8) with $u(x) = u_l(x)$, which is the total field corresponding to $u^i(x; d_l, k)$. Thus, by the definition of H_m in (2.5), we have

$$H_m\left(U'_l(\partial D)(\theta)\right) = C_N \int_{\partial K_R} \left\{ v_{\theta,l}(y)\frac{\partial e^{-ik\hat{x}_m \cdot y}}{\partial \nu(y)} - \frac{\partial v_{\theta,l}}{\partial \nu}(y)e^{-ik\hat{x}_m \cdot y} \right\} ds(y), \quad \hat{x}_m \in \mathbb{S}^{N-1}. \tag{3.14}$$

Insert (3.14) into (3.13), and use the definition of w^i_l and R_{lm} given in (3.12), we have

$$\begin{aligned}
J'(\partial D)(\theta) &= \frac{1}{LM}\mathfrak{R}\sum_{l=1}^{L}\sum_{m=1}^{M} R_{lm}(\partial D)C_N \int_{\partial K_R} \left\{ v_{\theta,l}(y)\frac{\partial e^{-ik\hat{x}_m \cdot y}}{\partial \nu(y)} - \frac{\partial v_{\theta,l}}{\partial \nu}(y)e^{-ik\hat{x}_m \cdot y} \right\} ds(y) \\
&= \frac{1}{L}\mathfrak{R}\sum_{l=1}^{L}\int_{\partial K_R} \left\{ v_{\theta,l}(y)\frac{\partial w^i_l}{\partial \nu}(y) - \frac{\partial v_{\theta,l}}{\partial \nu}(y)w^i_l(y) \right\} ds(y).
\end{aligned} \tag{3.15}$$

Using the Green's theorem for $v_{\theta,l}$ and w^i_l in $K_R \setminus \overline{D}$ implies that

$$\int_{\partial K_R} \left\{ v_{\theta,l}(y)\frac{\partial w^i_l}{\partial \nu}(y) - \frac{\partial v_{\theta,l}}{\partial \nu}(y)w^i_l(y) \right\} ds(y) = \int_{\partial D} \left\{ v_{\theta,l}(y)\frac{\partial w^i_l}{\partial \nu}(y) - \frac{\partial v_{\theta,l}}{\partial \nu}(y)w^i_l(y) \right\} ds(y). \tag{3.16}$$

Similarly, using the Green's theorem for the radiating solution $v_{\theta,l}$ and w^s_l in $K_{\tilde{R}} \setminus \overline{D}$, and letting $\tilde{R} \to \infty$ implies that

$$\int_{\partial D} \left\{ v_{\theta,l}(y)\frac{\partial w^s_l}{\partial \nu}(y) - w^s_l(y)\frac{\partial v_{\theta,l}}{\partial \nu}(y) \right\} ds(y) = 0. \tag{3.17}$$

Putting (3.16) and (3.17) into (3.15), together with $w^i_l + w^s_l = 0$ on ∂D, we have

$$\begin{aligned}
J'(\partial D)(\theta) &= \frac{1}{L}\mathfrak{R}\sum_{l=1}^{L}\int_{\partial D} \left\{ v_{\theta,l}(y)\frac{\partial w^i_l}{\partial \nu}(y) - \frac{\partial v_{\theta,l}}{\partial \nu}(y)w^i_l(y) \right\} ds(y) \\
&= \frac{1}{L}\mathfrak{R}\sum_{l=1}^{L}\int_{\partial D} \left\{ v_{\theta,l}(y)\frac{\partial w^i_l}{\partial \nu}(y) + \frac{\partial v_{\theta,l}}{\partial \nu}(y)w^s_l(y) \right\} ds(y) \\
&= \frac{1}{L}\mathfrak{R}\sum_{l=1}^{L}\int_{\partial D} \left\{ v_{\theta,l}(y)\frac{\partial w^i_l}{\partial \nu}(y) + v_{\theta,l}\frac{\partial w^s_l}{\partial \nu}(y) \right\} ds(y) \\
&= \frac{1}{L}\mathfrak{R}\sum_{l=1}^{L}\int_{\partial D} \frac{\partial u_l}{\partial \nu}\frac{\partial w_l}{\partial \nu}(\nu \cdot \theta)\, ds.
\end{aligned}$$

This completes the proof. $\qquad\qquad\qquad\qquad\qquad\qquad\qquad\qquad\qquad\qquad\qquad\qquad\qquad\qquad\quad\square$

Remark 3.3. *From the explicit form of the shape derivative of the cost functional J given in (3.10), one observes that choosing the perturbation θ such that*

$$\theta = -\Delta t\frac{1}{L}\mathfrak{R}\sum_{l=1}^{L}\frac{\partial u_l}{\partial \nu}\frac{\partial w_l}{\partial \nu}\nu =: -\Delta t\, v_D\, \nu \quad \text{on} \quad \partial D \tag{3.18}$$

for some descent step $\Delta t > 0$ yields

$$J(\partial D_\theta) = J(\partial D) - \Delta t \int_{\partial D} |\mathrm{v}_D|^2 ds + o(\Delta t) < J(\partial D),$$

for t sufficiently small. The function $\mathrm{v}_D \nu$ can be formally interpreted as the $L^2(\partial D)$ gradient of the functional J. Remark that for these calculations to be compatible with the statement of our theorem, v_D should be a C^1 function, which is not guaranteed if ∂D in only a C^2 boundary. We refer to the regularization section below for a possible way to fix this issue.

Remark 3.4. *According to (3.11), the adjoint state w_l solves the same scattering problem as u_l with an incident field being a linear combination of plane waves in the directions $-\hat{x}_m$, $m = 1, \ldots, M$. Therefore, if those directions are included in the set of incident directions d_l, $l = 1, \ldots, L$, the computation of the adjoint field does not require additional resolutions of the scattering problem but only a linear combination of previously computed fields.*

3.3 Explicit shape derivatives various data settings

We shall explicit the cost functional and the incident field for the adjoint state in the following three types of data settings: far field data, backscattering data and phaseless data.

3.3.1 Far field data

For the far field measurement case, the function ϕ in (2.6) is chosen to be $\phi(z) = z$, that is,

$$\phi\left(H_m u_l^s(\partial D)\right) = H_m u_l^s(\partial D) := u_D^\infty(\hat{x}_m, d_l).$$

Here $u_D^\infty(\hat{x}_m, d_l)$ refers to the far field of the scattered field $u_l^s(\partial D)$ which is the solution to (2.2) at the measured direction $\hat{x}_m$. The exact expression for the cost functional is

$$J_1(\partial D) := \frac{1}{2LM} \sum_{l=1}^{L} \sum_{m=1}^{M} \left| u_D^\infty(\hat{x}_m, d_l) - u_{D^\star}^\infty(\hat{x}_m, d_l) \right|^2. \tag{3.19}$$

By (3.12), the incident wave $w_{l,1}^i$ for the adjoint problem (3.11) is

$$w_{l,1}^i(y) := \frac{C_N}{M} \sum_{m=1}^{M} \overline{\left(u_D^\infty(\hat{x}_m, d_l) - u_{D^\star}^\infty(\hat{x}_m, d_l) \right)} e^{-ik\hat{x}_m \cdot y}. \tag{3.20}$$

3.3.2 Backscattering far field data

Backscattering refers that for each incident direction d, we only measure the far field data u^∞ at direction $-d$. Then from (3.19) and (3.20), set $M = 1$ and $\hat{x}_m = -d_l$, we get the exact expression for the cost function

$$J_2(\partial D) := \frac{1}{2L} \sum_{l=1}^{L} \left| u_D^\infty(-d_l, d_l) - u_{D^\star}^\infty(-d_l, d_l) \right|^2, \tag{3.21}$$

9

and the incident wave $w_{l,2}^i$ for the adjoint problem (3.11) is

$$w_{l,2}^i(y) := C_N \overline{\left(u_D^\infty(-d_l, d_l) - u_{D\star}^\infty(-d_l, d_l)\right)} e^{ikd_l \cdot y}.$$

Observe that in this case the incident field for the adjoint problem is proportional to the incident field for the forward problem. Suppose that u_l is the total field for the scattering problem (2.2) with $d = d_l$, then the solution $w_{l,2}$ of (3.10) with $w_l^i = w_{l,2}^i$ is

$$w_{l,2} := C_N \overline{\left(u_D^\infty(-d_l, d_l) - u_{D\star}^\infty(-d_l, d_l)\right)} u_l.$$

Thus, the descent direction $v_D = v_{D,2}$ as defined in Remark 3.3 can be directly computed as

$$v_{D,2} = \frac{C_N}{L} \Re \sum_{l=1}^{L} \overline{\left(u_D^\infty(-d_l, d_l) - u_{D\star}^\infty(-d_l, d_l)\right)} \left(\frac{\partial u_l}{\partial v}\right)^2.$$

3.3.3 Phaseless data

In many practical applications, the phase of the far-field pattern can not be measured accurately compared with its modulus or intensity and sometimes is even impossible to be measured, and therefore it is often desirable to reconstruct the scattering obstacle from phaseless data. The real-valued function ϕ corresponding to this case is

$$\phi(z) = \frac{|z|^2}{\sqrt{|z|^2 + \epsilon}}, \tag{3.22}$$

where $\epsilon > 0$ is a small constant to ensure differentiability of the cost functional. The expression for the cost functional with phaseless data can be written as

$$J_3(\partial D) := \frac{1}{2LM} \sum_{l=1}^{L} \sum_{m=1}^{M} \left| \frac{\left|u_D^\infty(\hat{x}_m, d_l)\right|^2}{\sqrt{\left|u_D^\infty(\hat{x}_m, d_l)\right|^2 + \epsilon}} - \frac{\left|u_{D\star}^\infty(\hat{x}_m, d_l)\right|^2}{\sqrt{\left|u_{D\star}^\infty(\hat{x}_m, d_l)\right|^2 + \epsilon}} \right|^2. \tag{3.23}$$

By (3.12), the incident wave $w_{l,3}^i$ for the adjoint problem (3.11) is

$$w_{l,3}^i(y) := \frac{C_N}{M} \sum_{m=1}^{M} \overline{\left(\phi(u_D^\infty(\hat{x}_m, d_l)) - \phi(u_{D\star}^\infty(\hat{x}_m, d_l))\right) \frac{|u_D^\infty(\hat{x}_m, d_l)|^2 + 2\epsilon}{(|u_D^\infty(\hat{x}_m, d_l)|^2 + \epsilon)^{3/2}} u_D^\infty(\hat{x}_m, d_l)} e^{-ik\hat{x}_m \cdot y}.$$

4 The Accelerated Level-Set Algorithm

Level-set methods are a famous and by now widely used conceptual framework where level-sets are employed as a tool for numerical analysis of surfaces and shapes. The advantage of the level-set model is that one can perform numerical computations involving curves and surfaces on a fixed Cartesian grid G without having to parameterize these objects (actually G could also be a mesh).

For the inverse scattering problem at hand, we want to reconstruct the unknown objects using a gradient descent scheme. Compared to the boundary variation method, the level-set method makes it easy to follow shapes that change topology during iterations, for example, when a connected shape splits into two, develops holes, or the reverse of these operations. This allows us not need to know the number of connected components in advance. This advantage makes it very convenient to real applications.

For a boundary ∂D of domain D, a level set function associated with this boundary is a continuous function defined on $\mathbb{R}^N$ such that

$$\partial D = \{x \in \mathbb{R}^N \mid \varphi(x) = 0\} \quad \text{and} \quad D = \{x \in \mathbb{R}^N \mid \varphi(x) < 0\}.$$

For instance, a signed distance function d_D defined as:

$$d_D(x) = \begin{cases} -d(x, \partial D) & \text{if} \quad x \in D, \\ 0 & \text{if} \quad x \in \partial D, \\ d(x, \partial D) & \text{if} \quad x \in \mathbb{R}^N \backslash \overline{D}. \end{cases}$$

where $d(\cdot, \partial D)$ is the usual Euclidean distance function to ∂D:

$$d(x, \partial D) := \inf_{y \in \partial D} |x - y|$$

is an example of a level set function associated with ∂D. If the curve ∂D regularly depends on a (pseudo) time parameter t and moves in the normal direction with a speed v, then a regular level-set function φ associated with ∂D satisfies the Hamilton-Jacobi equation [33, 38]

$$\frac{\partial \varphi}{\partial t} + v|\nabla \varphi| = 0. \tag{4.24}$$

For given v, equation (4.24) is usually numerically approximated on a cartesian gird (that can be independent from the grid or mesh used for computing the solution to the scattering problem). The design of stable numerical schemes for the level-set equation requires sophisticated techniques. Simple finite-differences methods may quickly fail. We refer to [16] for discussions of advanced numerical methods that efficiently handle this problem. We shall rely on the toolbox [28] in our numerical implementation of the inverse solver developed below.

The first step for application of the level set method to our problem is the definition of the velocity field v.

4.1 Regularized velocity field for the level set equation

According to Remark 3.3, a natural choice for v would correspond with $v = v_D$ on ∂D. Since we added no regularization term to the cost functional, this choice may produce a very irregular descent directions and prevent convergence by creating distorted shapes [21]. This is why it is often necessary to smooth this descent direction so that the shapes stay regular during iterations. One then should additionally define an extension of this velocity field to the whole computational domain of the level set function. There

are several possibilities to do the velocity regularization/extension based on solving a Laplacian problem [1]. Inspired by the solution to the forward problem, we here propose a slightly different approach that performs regularization and extension at the same time and also lead to an automatic calibration of the regularization parameter in terms of the frequency.

Theorem 4.1. *Let ∂D be of class C^2 and v_D be defined by (3.18). We define the regularized velocity v_{reg} as*

$$v_{\text{reg}}(x) := \int_{\partial D} G_{ik_r}(x, y) v_D(y) ds(y), \quad x \in \partial D, \tag{4.25}$$

where $k_r > 0$ is a regularizing parameter. Then $-\Delta t\, v_{\text{reg}} v \in C^1(\partial D, \mathbb{R}^N)$ and is a descent direction for $J(\partial D)$ for Δt sufficiently small.

Proof. From regularity properties of the exterior Dirichlet to Neumann operator for the exterior scattering problem [12, Theorem 3.13], one has that $v_D \in C^{0,\alpha}(\partial D)$ with $0 < \alpha < 1$. Consequently, from single layer potential regularity properties on Hölder spaces [12, Theorem 3.3], $v_{\text{reg}} \in C^{1,\alpha}(\partial D)$. Therefore $\theta := -\Delta t v_{reg} v \in C^1(\partial D, \mathbb{R}^N)$, and we have, using Theorem 3.2 and the definition of shape differentiation,

$$J(\partial D_\theta) - J(\partial D) = -\Delta t \int_{\partial D} v_D v_{\text{reg}}\, ds + o\,(\Delta t)\,.$$

From [12, Lemma 5.37] (see also Remark 4.2) the single layer potential $S_{k_r} : v_D\big|_{\partial D} \to v_{reg}\big|_{\partial D}$ is self-adjoint with respect to $L^2(\partial D)$ and is coercive with respect to $H^{-1/2}(\partial D)$ norm. Since v_D is a real valued function, this implies

$$\int_{\partial D} v_D v_{\text{reg}}\, ds \geq c_0 \|v_D\|^2_{H^{-1/2}(\partial D)}$$

for some positive constant c_0. Therefore, if $J'(\partial D) \neq 0$,

$$J(\partial D_\theta) - J(\partial D) \leq -\Delta t c_0 \|v_D\|^2_{H^{-1/2}(\partial D)} + o\,(\Delta t) < 0$$

for a Δt small enough. This shows that θ is a descent direction and completes the proof. $\quad\square$

A natural extension or the regularized velocity field v_{reg} to $\mathbb{R}^N$ that can be used for the level set equation is indeed

$$v_{\text{ext}}(x) := \int_{\partial D} G_{ik_r}(x, y) v_D(y)\, ds(y), \qquad x \in \mathbb{R}^N. \tag{4.26}$$

As can be observed below, k_r can be seen a parameter that adjust the spacial spread of the regularized and extended speed. We numerically observed that choosing $k_r = k$ yield good reconstruction accuracy and performances of the inversion algorithm.

12

Remark 4.2. *Using properties of single layer potentials with purely imaginary wave number one can observe that the extension defined by (4.26) verifies* $v_{ext} \in H^1(\mathbb{R}^N)$ *and is the unique solution to*

$$
\begin{aligned}
-\Delta v_{ext} + k_r^2 v_{ext} &= 0 \quad in \quad \mathbb{R}^N \backslash \partial D, \\
(\nabla v_{ext}^+ - \nabla v_{ext}^-) \cdot \nu &= -v_D \quad on \quad \partial D.
\end{aligned}
\tag{4.27}
$$

Moreover, $v_{ext} = v_{reg}$ *on* ∂D *and by the Green theorem*

$$
\int_{\partial D} v_D v_{reg} \, ds = \int_{\mathbb{R}^N} |\nabla v_{ext}|^2 + k_r^2 |v_{ext}|^2 dx.
$$

From (4.27), we observe that the single layer potential extension (4.26) is similar to smoothing based on diffusion kernels, with $1/k_r^2$ *being the regularization parameter. The main advantage of this regularization is that it does not require a prior smoothing or extension (like narrow band extension in [15]) of the shape gradient nor the addition of boundary conditions on the level set domain. We numerically observed that taking* $k_r = k$ *gives good results, which saves efforts to adjust this parameter for each example.*

4.2 Description of the accelerated level-set scheme

In this subsection, we present an accelerated level-set method to solve a shape optimization problem based on the previous analysis. We start by presenting the non accelerated scheme which is summarized in Algorithm 1. This algorithm consists in interpreting a gradient descent iteration with step Δt as advancing in time the solution of the Hamilton-Jacobi equation by a step Δt keeping fixed the velocity $v = v_{ext}$ defined by (4.26) associated with v_D from previous step.

The first main drawback of this algorithm is inherited from shortcoming of gradient descent algorithms for large set of parameters, i.e. the slow rate of convergence. In addition, we usually observe that although allowed in theory, the numerical algorithm does not allow for increasing the number of connected components during iterations. This may render the algorithm more sensitive to local minimum. This topology simplification during iterations may be made worse by the employed step adaptation, since we start with Δt^0 sufficiently large to avoid sensitivity to small oscillations of the cost functional.

Since the seminal work by Nesterov [31], it is well known that an efficient way to accelerate first order gradient descent schemes is to use combinations of previous steps. We recall in the following variant [7] that we would like to apply in the present work. Consider the optimization problem for a convex and regular function f

$$
\min_{x \in \mathbb{R}^N} f(x).
$$

We define the following sequence:

$$
\lambda_0 = 0, \quad \lambda_n = \frac{1 + \sqrt{1 + 4\lambda_{n-1}^2}}{2}, \quad \text{and} \quad \gamma_n = \frac{1 - \lambda_n}{\lambda_{n+1}}.
\tag{4.28}
$$

13

Algorithm 1 Non accelerated level-set inversion scheme

Initialization: Given a fixed Cartesian grid G and a step size value $\Delta t^0 > 0$, start from an initial signed distance function φ^0 corresponding to D^0 defined on G,

for $n = 0, 1, ..., Nit$, **do**

   1   Solve the direct scattering problem and the corresponding adjoint problem to get $\partial_\nu u_l^n$ and
        $\partial_\nu w_l^n$ on the zero-level set of φ^n and calculate J_n.

   2   Compute the velocity v_{D^n} on ∂D^n thanks to formula (3.18) and use (4.26) to compute the
        velocity extension $\mathrm{v}_{\mathrm{ext}}^n$ on the whole grid G.

        Set $T = \Delta t^0$.

   3   Solve the Hamilton-Jacobi equation

$$\begin{cases} \frac{\partial \varphi}{\partial t}(t, x) + \mathrm{v}_{\mathrm{ext}}^n(x)|\nabla \varphi(t, x)| = 0 & \text{on} \quad (0, T) \times G, \\ \varphi(t = 0, x) = \varphi^n(x) & \text{for} \quad x \in G. \end{cases}$$

        to get a level-set function $\varphi^{n+1}(x) = \varphi(T, x)$.

   4   Solve the direct scattering problem on the zero-level set of φ^{n+1} and calculate J_{n+1}.
        if $J_{n+1} < J_n$ **then**
           Go forward to step 5.
        else if $T > tol$ *(step tolerance)* **then**
           Set $T = 0.5\,T$ and go back to step 3.
        else
           Stop and quit the program.
        end if

   5   Redistance φ^{n+1} as a signed distance function (this step is only required if the level set varia-
        tions are too small compared to the grid mesh size).

end for

(Note that $-1 \le \gamma_n \le 0$ for $n > 0$). An accelerated gradient scheme can be written as follows, with $x_1 = y_1$ being an arbitrary initial point,

$$
\begin{aligned}
y_{n+1} &= x_n - t^n \nabla f(x_n), \\
x_{n+1} &= (1 - \gamma_n) y_{n+1} + \gamma_n y_n.
\end{aligned}
$$

The convergence result for this algorithm can be found in [9].

The main difficulty in applying this idea to Algorithm 1 is to properly define combinations of level sets that would coincide with the same combinations of boundaries (with respect to a given definition of a metric on the set of admissible boundaries). Let us for instance remark that if the boundary is parametrized with a fixed set of basis functions (which is for instance the employed strategy for star like geometries), then there is no difficulty in transposing the accelerated scheme to that setting by taking x_n to be the coordinates of the geometry parametrization in the chosen basis. However, if one replaces x_n with φ^n then there is no clear link between the resulting scheme and the one applied to x_n. If φ^n coincides with the signed distance function, then one can establish this link in the simplified one dimensional setting as explained below.

Suppose that we have two one dimensional signed distance functions ψ^n and ψ^{n+1} as shown in Figure 1 where the boundaries defined by these level set functions are respectively $\{y_n^1, y_n^2\}$ and $\{y_{n+1}^1, y_{n+1}^2\}$ with $y_\ell^1 < y_\ell^2$. Let us define a new level-set function φ^{n+1} as

$$
\varphi^{n+1} = (1 - \gamma_n) \psi^{n+1} + \gamma_n \psi^n. \tag{4.29}
$$

One easily guess from Figure 1 that if ψ^{n+1} is sufficiently close to ψ^n, then in the neighborhood of the zeros ψ^{n+1} and ψ^n are affine functions with the same slope and consequently the zeros of φ^{n+1} are

$$
x_{n+1}^j = (1 - \gamma_n) y_{n+1}^j + \gamma_n y_n^j, \quad j = 1, 2. \tag{4.30}
$$

More precisely, in order to ensure that x_{n+1}^1 is a zero of φ^{n+1}, it is sufficient to ensure that

$$
x_{n+1}^1 < min(\tilde{y}_n, \tilde{y}_{n+1}) \tag{4.31}
$$

with $\tilde{y}_\ell = (y_\ell^1 + y_\ell^2)/2$, which means that x_{n+1}^1 indeed lies in a region where ψ^{n+1} and ψ^n have the same slope. In the case $y_{n+1}^1 \le y_n^1$, $x_{n+1}^1 = y_{n+1}^1 + \gamma_n(y_n^1 - y_{n+1}^1) < y_{n+1}^1$ since $\gamma_n \le 0$ and therefore (4.31) is verified. If $y_{n+1}^1 > y_n^1$, then, since $0 \ge \gamma_n \ge -1$, one can easily check that (4.31) is verified as long as

$$
y_{n+1}^1 - y_n^1 < min((y_n^2 - y_n^1)/4, (y_{n+1}^2 - y_{n+1}^1)/2). \tag{4.32}
$$

Symmetrically, (replace $\psi^\ell(y)$ by $\psi^\ell(-y)$), x_{n+1}^2 is a zero of φ^{n+1} if

$$
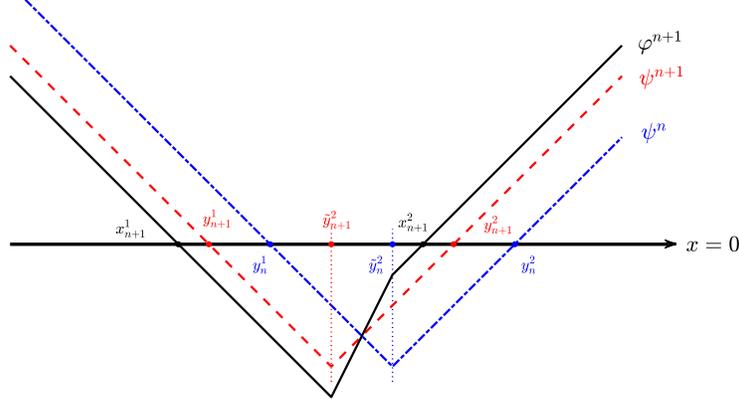y_n^2 - y_{n+1}^2 < min((y_n^2 - y_n^1)/4, (y_{n+1}^2 - y_{n+1}^1)/2). \tag{4.33}
$$

15

Figure 1: Combination of two one-dimensional signed distance functions ψ^n and ψ^{n+1}.

Conditions (4.32) and (4.33) can be interpreted as a condition on Δt being sufficiently small so that the gradient descent increment is sufficiently small compared to the size of the domain. These observations on the one dimensional case motivated the accelerated scheme proposed in Algorithm 2. In this algorithm, the main additional step is to transform the solution of the Hamilton-Jacobi equation into a signed distance function, then compute the updated level set function using (4.29). The rationality behind this scheme is that in higher dimensions, since we locally vary the boundary along the normal, assuming that the changes in the normal is of higher order with respect to the gradient descent step, locally the signed distance functions behave as in the 1D example, where the coordinate system represents the axis along the normal.

As indicated in the introduction, the present article can be viewed as a proof of concept with only numerical validations for the proposed algorithm. The convergence analysis is still under progress in the case of convexity assumptions on the cost functional (although this is not guaranteed in general for inverse scattering problems).

5   Numerical results

In this section, several numerical examples are carried out to show the effectiveness of the regularized level-set method and compare the convergence speed of our accelerated level-set method with the non accelerated scheme. We use the gypsilab toolbox [2] to solve the direct scattering problems. To solve the Hamilton-Jacobi equation, we use the matlab level set toolbox [28]. More precisely, we use the algorithm referred to *Motion in the Normal Direction* presented in [28, Section 2.3, equation (7)]. For redistancing, we use [28, Section 2.3, equation (8)].

The following items are shared by all numerical examples.

(1) To generate the synthetic data we use the gypsilab toolbox [2] to solve the direct scattering problem for the exact shapes. The noise level $\delta = 5\%$ and the noisy data $\tilde{u}_\delta$ is computed from the exact one

---

Algorithm 2 Accelerated level-set scheme

Initialization: Given a fixed Cartesian grid G and a step size value $\Delta t^0 > 0$, start from an initial signed distance function φ^0 corresponding to D^0 defined on G,

for $n = 0, 1, ..., Nit$, **do**

    1   Solve the direct scattering problem and the corresponding adjoint problem to get $\partial_\nu u_l^n$ and $\partial_\nu w_l^n$ on the zero-level set of φ^n and calculate J_n.

    2   Compute the velocity v_{D^n} on ∂D^n thanks to formula (3.18) and use (4.26) to compute the velocity extension v_{ext}^n on the whole grid G.

        Set $T = \Delta t^0$.

    3   Solve the Hamilton-Jacobi equation

$$\begin{cases} \frac{\partial \varphi}{\partial t}(t, x) + v_{ext}^n(x)|\nabla \varphi(t, x)| = 0 & \text{on} \quad (0, T) \times G, \\ \varphi(t = 0, x) = \varphi^n(x) & \text{for} \quad x \in G. \end{cases}$$

        to get a level-set function $\varphi^{n+1}(x) = \varphi(T, x)$.

    4   Solve the direct scattering problem on the zero-level set of φ^{n+1} and calculate $\widetilde{J}_{n+1}$.

        if $\widetilde{J}_{n+1} < J_n$ **then**

            Go forward to step 5.

        else if $T > tol$ *(step tolerance)* **then**

            Set $T = 0.5\,T$ and go back to step 3.

        else

            Stop and quit the program.

        end if

    5   Redistance φ^{n+1} as a signed distance function to get a new function ψ^{n+1}

    6   Compute the new update for the level set function as

$$\varphi^{n+1} \quad = \quad (1 - \gamma_n)\,\psi^{n+1} + \gamma_n \psi^n$$

        where γ_n is the sequence defined by (4.28).

end for

$\tilde{u}$ using the formula $\tilde{u}_\delta = \tilde{u}(1 + \delta\eta)$, where η is a normally distributed random number in $[-1, 1]$ and $\tilde{u} := u_\infty$ for far field pattern or $\tilde{u} := |u_\infty|$ for phaseless data.

(2) The computational region for the level set functions is chosen to be a square with side length 10 centered at $(0, 0)$. This region is discretized using a cartesian grid with steps $\Delta x = \Delta y = 0.04$.

(3) The wave number of the incident wave is chosen to be $k = 1$ unless otherwise stated. For the parameters in the inversion algorithm, we choose an initial step size $\Delta t^0 = 2$ and a regularization parameter $k_r = k$.

(4) For far field and phaseless data, we transmit $L = 36$ equidistant incident plane waves on a full aperture and evaluate $M = 36$ equidistant measurements on a full aperture for each incident wave. For back-scattering data, we transmit $L = 360$ equidistant incident plane waves on a full aperture and evaluate the far field at $-d_l$ for each incident direction d_l.

(5) In each example, in addition to showing the final reconstruction results, we compare the decay rate of the cost functional between Algorithm 1 and Algorithm 2. For the n-th iteration, we calculate $\log_{10}(J_n/J_o)$ with $J_n = J(\partial D^n)$ and J_o being the value of J corresponding to $\phi = 0$ (see (2.6)).

Remark 5.1. *Although the step adaptation is incorporated in the accelerated scheme, we observe that it does not imply that the cost functional is always decreasing. This is what is also numerically observed in the results below. In fact, for the value of Δt^0 chosen above, the adaptation step was never activated by Algorithm 2 in the experiments below while it was sometimes activated by Algorithm 1.*

We consider the following three configurations. Configuration 1 includes a kite-shaped obstacle located at $(-\sqrt{2}, \sqrt{2})$ and it is described by the parametric representation

$$x_{kite}(t) = \left(-\sqrt{2} + (0.75\cos t + 0.5\cos 2t - 0.5), \sqrt{2} + \sin t\right), \quad 0 \le t \le 2\pi.$$

In configuration 2, we add an ellipse located at $(\sqrt{2}, -\sqrt{2})$ to the kite-shaped obstacle. The ellipse is defined by

$$x_{ellipse}(t) = \left(\sqrt{2} + \frac{1.5\cos t}{\sqrt{\sin^2 t + 2.25\cos^2 t}}, -\sqrt{2} + \frac{1.5\sin t}{\sqrt{\sin^2 t + 2.25\cos^2 t}}\right), \quad 0 \le t \le 2\pi.$$

In configuration 3, we consider a whale-shaped obstacle for which the exact boundary can not be globally parametrized as for the previous examples. The three configurations are depicted in Figure 2.

For each configuration, the following three different initial guesses are tested:

(1) One circle with radius $R = 1$ located at $(0, 0)$;

(2) Two circles with radius $R = 1$ located at $(0, 0)$ and $(-2.5, 0)$;

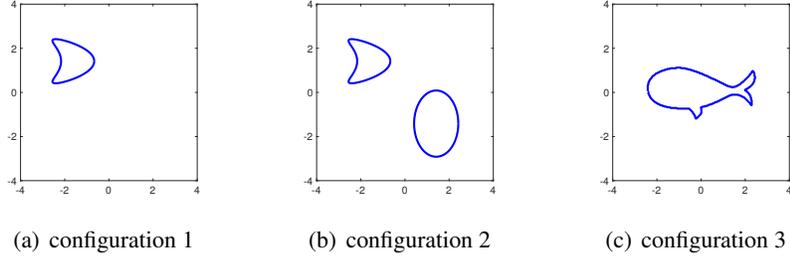(3) Three circles with radius $R = 1$ located at $(0, 0)$, $(-2.5, 0)$ and $(2.5, 0)$.

(a) configuration 1   (b) configuration 2   (c) configuration 3

Figure 2: The considered configurations for the domain *D*.

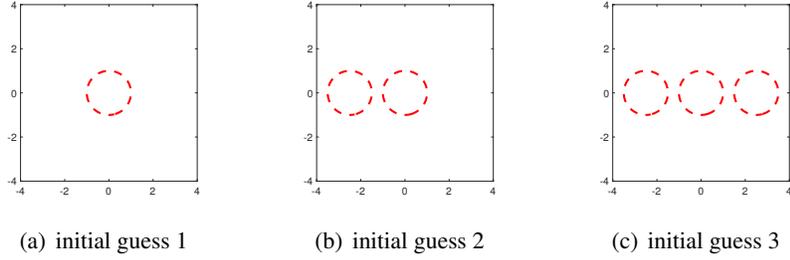(a) initial guess 1   (b) initial guess 2   (c) initial guess 3

Figure 3: Initial guesses.

These initial guesses are depicted in Figure 3.

Example 1: Shape reconstruction with far field data. We first consider the inverse problem with far field data generated by configuration 1, which includes only one kite-shaped obstacle. The reconstructions due to different initial guesses are presented in Figure 4. In Figure 4(a)-(d), the results show that both algorithms converge to the exact boundary and our accelerated method converges faster. In Figure 4(e)-(h) and Figure 4(i)-(l), Algorithm 2 converges while Algorithm 1 stops since the cost functional cannot be further decreased (after the step size reached the lower tolerance). Therefore, the accelerated algorithm not only converges faster, but also can deal with the case in which the classical approach does not work. In other words, our method offers more flexibility for the choice of the initial guess, which may be useful for cases with no a priori information on the connectivity of the obstacle.

We second consider the inverse problem with far field measurements generated by configuration 2, which includes two obstacles: a kite-shaped obstacle and an ellipse. The reconstructed shapes associated with different initial guesses are presented in Figure 5. It can be seen that both algorithms converge no matter how many obstacles the initial guess includes, while the accelerated method converges faster and can provide a more accurate reconstruction of the exact curves.

Example 2: Shape reconstruction with back-scattering data. In this example, we discuss the inverse scattering problem using back-scattering measurements. First, we consider configuration 1 and initial guess 1 presented in Figure 4(a). The reconstructed results are shown in Figure 6. It can be seen that both algorithms do not converge to the exact boundary. In fact this is due to the non convexity of the cost functional in a neighborhood of the initial guess. In order to visualize this non convexity, we compute *J* for different shapes (circles) that depend on one parameter and plot the obtained function. In

(a) original and initial   (b) convergence speed   (c) Algorithm 1, *Nit* = 101   (d) Algorithm 2, *Nit* = 101

(e) original and initial   (f) convergence speed   (g) Algorithm 1, *Nit* = 35   (h) Algorithm 2, *Nit* = 101

(i) original and initial   (j) convergence speed   (k) Algorithm 1, *Nit* = 49   (l) Algorithm 2, *Nit* = 101
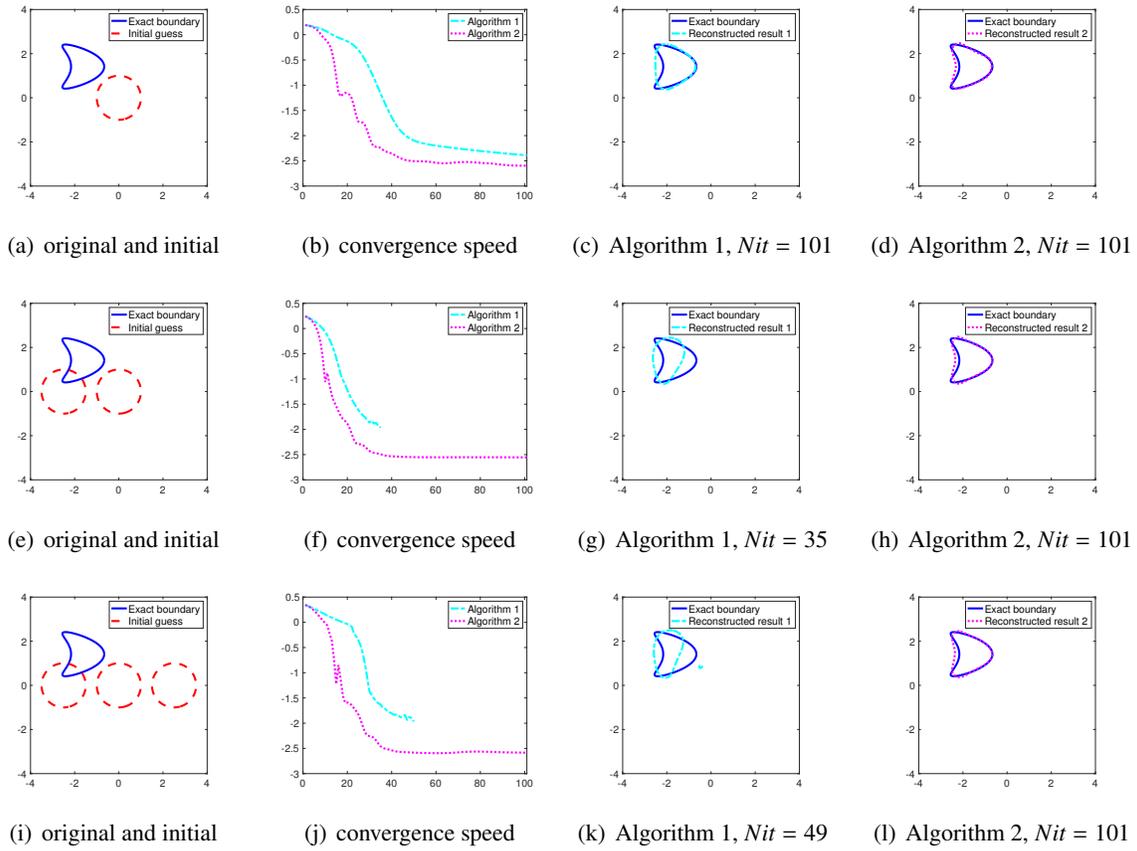
Figure 4: Shape reconstructions for configuration 1 using far field data with different initial guesses. The first column gives the profile of the exact boundary and the initial guess. The second column presents the convergence speed for the cost functional by Algorithm 1 (dashed line) and Algorithm 2 (dotted line). The third and fourth columns show the final reconstructions given by Algorithm 1 and Algorithm 2, respectively.

20

(a) original and initial (b) convergence speed (c) Algorithm 1, $Nit = 151$ (d) Algorithm 2, $Nit = 151$

(e) original and initial (f) convergence speed (g) Algorithm 1, $Nit = 151$ (h) Algorithm 2, $Nit = 151$

(i) original and initial (j) convergence speed (k) Algorithm 1, $Nit = 151$ (l) Algorithm 2, $Nit = 151$
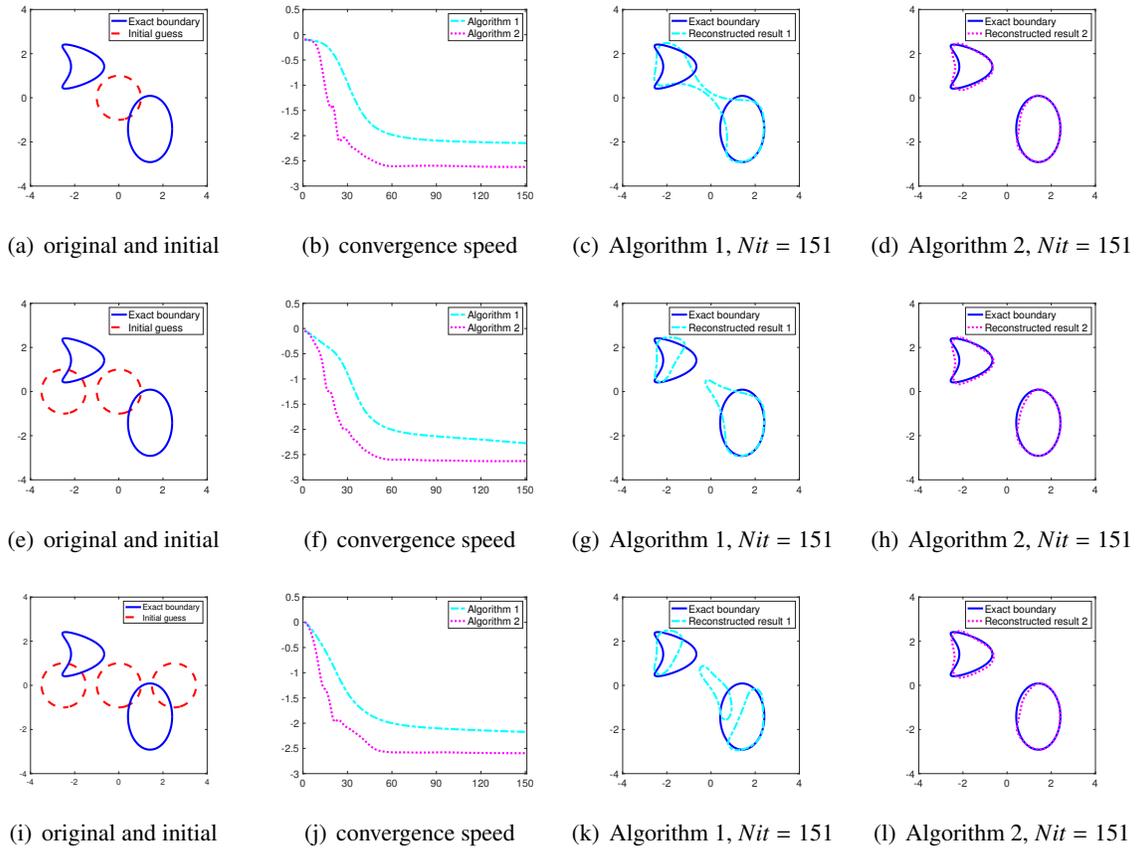
Figure 5: Shape reconstructions for configuration 2 using far field data with different initial guesses. The first column gives the profile of the exact boundary and the initial guess. The second column presents the convergence speed for the cost functional by Algorithm 1 (dashed line) and Algorithm 2 (dotted line). The third and fourth columns show the final reconstructions given by Algorithm 1 and Algorithm 2, respectively.

a first case we fix the center at $(0, 0)$ and change the radius of this circle from $R = 0.1$ to $R = 3$ (Figure 7 (a) and (b)). In a second case we fix the radius $R = 1$ and change the location of the center along the straight segment joining $(0, 0)$ to $(-\sqrt{2}, \sqrt{2})$ (Figure 7 (a) and (b)). For both cases we also compute the cost functional J corresponding with the full aperture far field data as in the Example 1 (depicted with dashed lines). Figures 7(b) and (d) clearly show a severe non convexity change of the cost functional associated with back-scattering data. Using the initial guess in Figure 6 made the accelerated algorithm trapped in a local minimum present in its neighborhood. It seems that for the full aperture case the non convexity change is much less severe and this is why the accelerated algorithm was more successful to escape local minima in that case.

By changing the initial guess, for instance using a circle located at $(-0.5, 0.5)$ with radius $R = 1$ as shown in Figure 8, both algorithms provide good reconstructions and the accelerated one exhibit a faster convergence as in the previous examples.
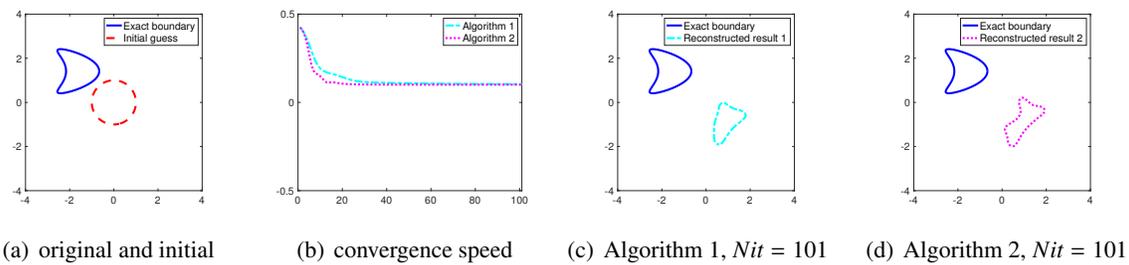

(a) original and initial   (b) convergence speed   (c) Algorithm 1, $Nit = 101$ (d) Algorithm 2, $Nit = 101$

Figure 6: Shape reconstructions for configuration 1 using back-scattering data with initial guess 1.

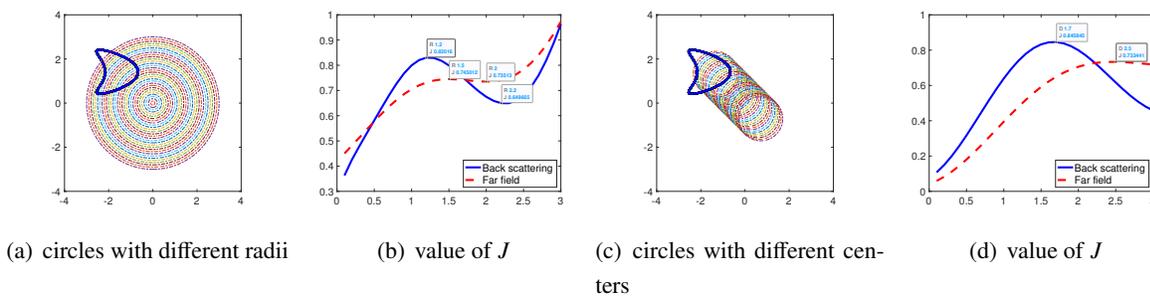(a) circles with different radii   (b) value of J (c) circles with different centers   (d) value of J

Figure 7: The value of the cost functional J for backscattering data (solid line) and full aperture data (dashed line) for exact data associated with kite-shape obstacle and for domains corresponding with circles of different radii or locations. In (a)-(b) we fix the center of the circles at $(0, 0)$ and change the radius of this circle from $R = 0.1$ to $R = 2$. In (c)-(d) we fix the radius $R = 1$ and change the location of the center along the straight segment joining $(0, 0)$ to $(-\sqrt{2}, \sqrt{2})$.

Example 3: Shape reconstruction with phaseless data. In this example, we consider configuration 2 for shapes with phaseless data [20], which has a more widely use in real applications. We remark that due to the translation invariance for phaseless data, one can only reconstruct the shapes up to a translation (but which is the same for all connected components). This compatible with the reconstructed results

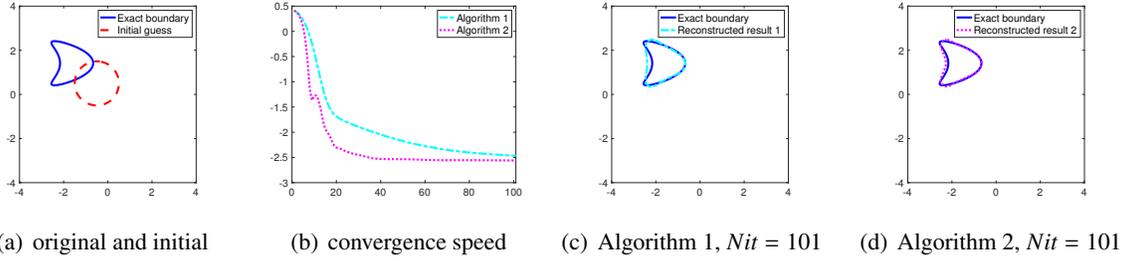(a) original and initial (b) convergence speed (c) Algorithm 1, *Nit* = 101 (d) Algorithm 2, *Nit* = 101

Figure 8: Shape reconstructions for configuration 1 using back-scattering data with an initial guess being a circle with radius $R = 1$ located at $(-0.5, 0.5)$.

shown in Figure 9. In all of the three cases, Algorithm 2 needs less than 200 steps of iterations while Algorithm 1 needs more than 1000 iterations before convergence. Moreover, Figure 9(i)-(l) shows that Algorithm 2 is more tolerant with the initial guess than Algorithm 1. It provides a good reconstruction after 200 iterations while Algorithm 1 does not perform well even after 1000 iterations.

Example 4: Shape reconstruction of configuration 3 with multi-frequency full aperture data. In this last experiment, we consider an object with a more complex geometry given by the whale-shaped obstacle. The exact boundary is approximated by 582 points. Due to this large number of parameters, and the difficulty to design a priori parametrization of the shape make gradient descent methods well suited optimization strategy for this case. Additionally since there are some small details in the geometry, we need to successively use data produced at higher frequencies to get better reconstructions (see [6]). This is what the numerical experiments in Figure 10 also suggest. At a low wave number $k = 1$ as used in the previous examples, the reconstructed shape misses the small details while the residual is small and cannot be improved by the algorithm: see Figure 10(a)-(d). Using a larger wave number, for example, $k = 5$ we observe that if we use the same initial guess as in the previous case, both algorithms get stuck into a local minimum see Figure 10(e)-(h). One can think in this case to use adaptation of the regularization strategy but we found it hard to automatically tune parameters in this case. This leads us to consider a multi-frequency strategy similar to [6]. We first use a low frequency incident waves to get a reconstruction at $k = 1$. Then we take it as the initial guess for higher wave number $k = 5$. The numerical results are shown in Figure 10(i)-(l) and shows that this type of strategy is successful. The accelerated algorithm still outperforms the non accelerated one.

6 Conclusion

We presented a new algorithm to solve inverse obstacle scattering problems based on an accelerated level-set approach. Since level-set functions allow for a larger variety of shapes, they usually induce more iterations than for boundary variation techniques. Motivated by accelerated gradient descent strategies that combine several iterates, we proposed an adaptation of these strategies to the level-set framework in order to reduce the number of iterations and accelerate the whole procedure. We also proposed

23

(a) original and initial   (b) convergence speed   (c) Algorithm 1, *Nit* = 1001   (d) Algorithm 2, *Nit* = 201

(e) original and initial   (f) convergence speed   (g) Algorithm 1, *Nit* = 1001   (h) Algorithm 2, *Nit* = 201

(i) original and initial   (j) convergence speed   (k) Algorithm 1, *Nit* = 1001   (l) Algorithm 2, *Nit* = 201
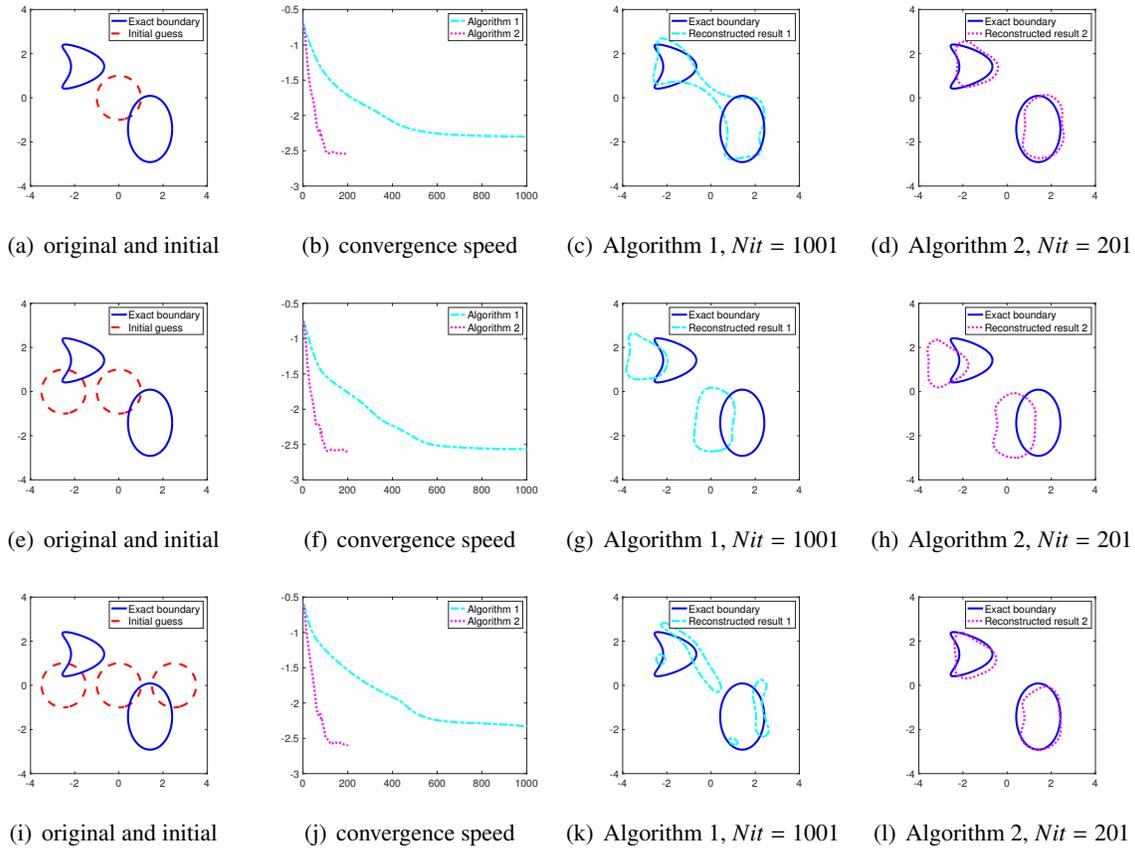
Figure 9: Shape reconstructions for configuration 2 using phaseless data with different initial guesses. The first column gives the profile of the exact boundary and the initial guess. The second column presents the convergence speed for the cost functional by Algorithm 1 (dashed line) and Algorithm 2 (dotted line). The third and fourth columns show the final reconstructions given by Algorithm 1 and Algorithm 2, respectively.

24

(a) original and initial

(b) convergence speed

(c) Algorithm 1, $Nit = 101$

(d) Algorithm 2, $Nit = 101$

(e) original and initial

(f) convergence speed

(g) Algorithm 1, $Nit = 101$

(h) Algorithm 2, $Nit = 101$

(i) original and initial

(j) convergence speed
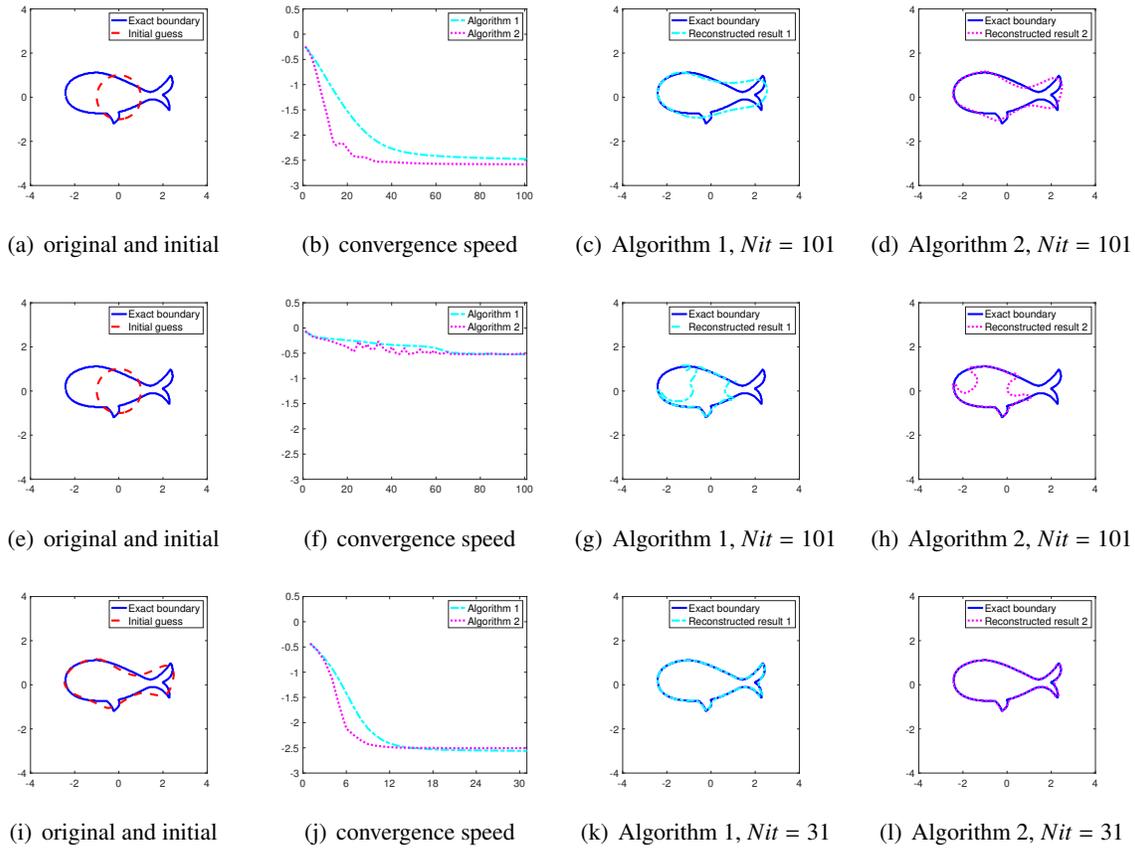
(k) Algorithm 1, $Nit = 31$

(l) Algorithm 2, $Nit = 31$

Figure 10: Shape reconstructions for configuration 3 using a multi-frequency full aperture data. The first row gives the results with the initial guess shown in (a) and the wave number $k = 1$ by Algorithm 1 and Algorithm 2. The second row gives the results with the initial guess shown in (e) and the wave number $k = 5$ by Algorithm 1 and Algorithm 2. The third row gives the results with the initial guess shown in (i), which is the final reconstruction given by a small wave number $k = 1$ (as shown in (c)), and then iterates with a larger wave number $k = 5$.

the use single-layer potentials to extend and regularize the descent direction given by the shape derivative. Numerical examples with different types of measurements have been conducted to demonstrate the expected superiority of the proposed approach over non accelerated approaches in terms of iterations number. They also demonstrated that the algorithm provides much more accurate reconstructions and is less sensitive to initial guesses (and the topology of both the initial guess and the reconstructed object). A theoretical analysis of these conclusions will be the subject of future works.

7   Acknowledgement

References

[1] G. Allaire, C. Dapogny and F. Jouve, Shape and topology optimization, in Geometric partial differential equations, part II, A. Bonito and R. Nochetto eds., *Handbook of Numerical Analysis* **22**, 1-132 (2021).

[2] F. Alouges and M. Aussal, FEM and BEM simulations with the Gypsilab framework, *SMAI-JCM* **4**, 297-318 (2018).

[3] H. Ammari, J. Garnier, H. Kang, M. Lim and K. Solna, Multistatic imaging of extended targets, *SIAM J. Imaging Sci.* **5**, 564-600 (2012).

[4] H. Ammari, J. Garnier, V. Jugnon and H. Kang, Stability and resolution analysis for a topological derivative based imaging functional, *SIAM J. Control Optim.* **50**, 48-76 (2012).

[5] L. Audibert and H. Haddar, A generalized formulation of the Linear Sampling Method with exact characterization of targets in terms of far field measurements, *Inverse Problems* **30**, 035011 (2014).

[6] G. Bao, P. Li, J. Lin and F. Triki, Inverse scattering problems with multi-frequencies, *Inverse Problems* **31**, 093001 (2015).

[7] A. Beck, M. Teboulle, A fast iterative shrinkage-thresholding algorithm for linear inverse problems. *SIAM J. Imaging Sci.* **2(1)**, 183-202 (2009).

[8] L. Bourgeois, N. Chaulet and H. Haddar, On Simultaneous Identification of the Shape and Generalized Impedance Boundary Condition in Obstacle Scattering, *SIAM Journal on Scientific Computing* **34**, A1824-A1848 (2012).

[9] S. Bubeck, Convex optimization: Algorithms and complexity, *Foundations and Trends in Machine Learning,* **8(3-4)**, 231-357 (2015).

[10] F. Cakoni, D. Colton and H. Haddar, *Inverse Scattering Theory and Transmission Eigenvalues*, SIAM publications, CBMS-NSF 88, 2016.

[11] G. Chavent, Identification of function parameters in partial differential equations, *Joint Automatic Control Conference*, New-York ASME (1974).

[12] D. Colton and R. Kress, *Inverse acoustic and electromagnetic scattering theory (3rd Ed.)*, Springer, Berlin, 2013.

[13] David Colton and Rainer Kress, Looking back on inverse scattering theory, *SIAM Rev.* **60(4)**, 779-807 (2018).

[14] O. Dorn and D. Lesselier, Level set methods for inverse scattering, *Inverse Problems* **22**, R67 (2006).

[15] O. Dorn and Y. Wu, Shape reconstruction in seismic full waveform inversion using a level set approach and time reversal, *Journal of Computational Physics*, 110059 (2020).

[16] D. Enright, R. Fedkiw, J. Ferziger, and I. Mitchell, A hybrid particle level set method for improved interface capturing, *J. Comput. Phys.,* **183(1)**, 83-116 (2002).

[17] F. Hettlich, Fréchet derivatives in inverse obstacle scattering, *Inverse Problems,* **11** , 371-382 (1995).

[18] T. Hohage, Convergence rates of a regularized Newton method in sound-hard inverse scattering, *SIAM J. Numer. Anal.* **36**, 125âĂŞ142 (1998).

[19] G. Incorvaia and O. Dorn, Stochastic Optimization Methods for Parametric Level Set Reconstructions in 2D through-the-Wall Radar Imaging, *Electronics*, **9(12)**, (2020).

[20] O. Ivanyshyn, Shape reconstruction of acoustic obstacles from the modulus of the far field pattern, *Inverse Probl. Imaging* **1**, 609-622 (2007).

[21] Z. Jiang, H. Haddar, A. Lechleiter and M. El-Guedri, Identification of magnetic deposits in 2-D axisymmetric eddy current models via shape optimization, *Inverse Problems in Science and Engineering* **24**, 1385-1410 (2016).

[22] A. Kirsch, The domain derivative and two applications in inverse scattering theory, *Inverse Problems,* **9**, 81-96 (1993).

[23] A. Kirsch and N. Grinberg, *The Factorization Method for Inverse Problems*, Oxford Univ. Press, Oxford, 2008.

[24] R. Kress, *Linear Integral Equations (3rd Ed.)*, Springer, Berlin, 2014.

[25] A. Lechleiter and A. Rieder, Towards a general convergence theory for inexact Newton regularizations, *Numerische Mathematik* **114**, 521–548 (2010).

[26] X. Liu, B. Zhang, Unique determination of a sound-soft ball by the modulus of a single far field datum, *J. Math. Anal. Appl.* **365**, 619-624 (2010).

[27] W. McLean, *Strongly Elliptic Systems and Boundary Integral Equations*, Cambridge University Press, Cambridge, 2000.

[28] I. Mitchell, The Flexible, Extensible and Efficient Toolbox of Level Set Methods, *Journal of Scientific Computing,* **35(2-3)**, 300-329 (2008).

[29] J.-C Nédélec, *Acoustic and Electromagnetic Equations*, Cambridge University Press. Springer, New York etc., 2001.

[30] Y. Nesterov, A method of solving a convex programming problem with convergence rate $O(1 \backslash k^2)$. *Soviet Mathematics Doklady,* **27**, 372-376 (1983).

[31] Y. Nesterov, *Lectures on Convex Optimization*, Springer, 2018.

[32] A. Neubauer, On nesterov acceleration for landweber iteration of linear ill-posed problems, *Journal of Inverse and Ill-posed Problem* **25(3)** (2016).

[33] S. Osher and R. Fedkiw, *Level set methods and dynamic implicit surfaces*, Springer-Verlag, New York, 2003.

[34] S. Osher and J. Sethian, Fronts propagating with curvature-dependent speed: algorithms based on Hamilton-Jacobi formulations, *J. Comput. Phys.,* **79(1)**, 12-49 (1988).

[35] R. Potthast, *Point Sources and Multipoles in Inverse Scattering Theory*, Chapman & Hall/CRC, Boca Raton, 2001.

[36] R. Potthast and I. Stratis, The singular sources method for an inverse transmission problem, *Computing* **75**, 237-255 (2005).

[37] F. Santosa, A level-set approach for inverse problems involving obstacles, *ESAIM: Control, Optimisation and Calculus of Variations* **1**, 17-33 (1996).

[38] J. Sethian, *Level set methods and fast marching method*, Cambridge University Press, Cambridge, second edition, 1999.

[39] A. Sommerfeld, Die Greensche Funktion der Schwingungsgleichung, *Jber. Deutsch. Math. Verein.,* **21**, 309-353 (1912).

[40] P. Tseng, Approximation accuracy, gradient methods, and error bound for structured convex optimization, *Math. Program., Ser. B* (2010).